
TEAM HYDRA II

Dual Colorimeter and pH Sensing System for
Ocean Exploration

Elijah Cole

Matthew Faw

Dean Hazineh

Tamra Nebabu

ECE 449 - SENSOR AND SENSOR INTERFACE DESIGN

Dr. Nan Jokerst, Dr. Martin Brooke

Duke University

April 27, 2017

Contents

1 Project Background	1
1.1 Objectives	1
1.2 Design Specifications	1
1.3 Project Management	2
1.4 Prototyping Costs and Bill of Materials	2
2 Theory of Sensor Operation	2
2.1 Colorimetry in Turbid Media	2
2.2 Electrochemical pH Sensing	4
3 Colorimetry	5
3.1 Capabilities	5
3.2 Demo Day Data	5
4 Turbidity	6
4.1 Preliminary Testing	6
4.2 Demo Day	6
5 pH Sensing	8
5.1 Preliminary Results and Challenges	8
5.2 Demo Day	10
6 Final Design Prototype	11
6.1 Colorimetric Sensor Design	12
6.2 Electrochemical Sensor Design	13

		3
6.3	Waterproofing	14
6.4	Environmental Impact	16
6.5	Comments on Design Challenges	17
7	Electronics and Power	18
7.1	Electronics Assembly and Design	18
7.2	SD Shield	19
7.3	Inductive Charging	19
7.4	Battery Life Estimation	20
8	Wireless Communication and Data Management	20
8.1	Motivation	20
8.2	Overview of Communication Model	20
8.2.1	Client-Server-Database Model	20
8.2.2	Server	21
8.2.3	Database	21
8.2.4	Router	22
8.2.5	Clients	22
8.3	Experiment Initiation, Monitoring, and Organization	23
8.4	Troubleshooting	23
8.4.1	Reliable data transfer	23
8.4.2	Memory limits	24
8.4.3	After closing the case	24
9	Conclusions	24

Appendix:

A Gantt Charts	26
B List of Expenses	26
C Documentation and Links	27

1 Project Background

1.1 Objectives

The purpose of this project is to design and build a fully-operational dual-sensing system which, when placed in the ocean, will measure the concentration of Rhodamine WT dye in the surrounding water, measure the pH via electrochemical sensing, and transmit the results wirelessly to a receiving computer. This project is motivated by the sensing challenges of the 2017 Shell Ocean Discovery XPRIZE, which is a global contest that encourages innovations in ocean engineering [1]. We note that although the project is motivated by the Ocean XPRIZE challenge, all testing and demonstrations of functionality will be completed in the laboratory utilizing samples and solutions which adequately mimic the physical conditions for ocean operation. In this report, we discuss the design of our system including its motivations, our initial test results, and our plans to complete this project.

1.2 Design Specifications

Because the sensing system discussed in this paper is our group's submission to the ECE 449 engineering design project, it is subject to additional constraints that we shall briefly review here. Our design is required to implement some form of optical colorimetry to evaluate the concentration of Rhodamine dye in the mock-up oceanwater samples. Specifically, our system must be able to distinguish *relative* concentrations of Rhodamine with a minimum resolution of 5 ppm, and be able to rank at least ten samples of unknown concentration between 0.1-10 $\mu\text{g}/\text{L}$. In addition, our colorimeter subsystem must be robust enough to perform the ranking regardless of the turbidity of the solutions, as the prepared samples will be infused with microspheres to simulate the turbid conditions of real oceanwater. All utilized concentration samples presented during the final demonstration will have turbidities ranging from 0.1-10 NTUs. In regards to pH sensing, our system must use metal electrodes as the pH probes, and the sensor design interface must be implemented utilizing the ADS1115 16-Bit 4 Channel ADC [2]. The performance requirements of the pH system include detecting pH in the range of 3-10 with an accuracy of 0.2 with respect to current gold-standard, commercial pH sensors.

There are also requirements associated with the auxiliary electronics for the sensor systems. First and foremost, the entire system must be fully powered by a 3.7 V Lithium-Ion battery. Furthermore, the power architecture of the system must allow for wireless inductive charging of the battery from *outside* the unit. The electronics must be implemented utilizing a soldered printed circuit board and the Adafruit Feather Huzzah [3] as the primary microcontroller. Alongside demonstrations which validate these aforementioned constraints, the final written report will include our design schematics and the results for analyses conducted on system power consumption, environmental impact, and the cost to

develop, scale, and manufacture.

In addition to the design constraints outlined above, our system must be able to overcome many of the practical challenges associated with ocean sensing systems. Because our system will be fully submerged in the final demonstration, the encasement for our electronics must be completely leak-proof. Furthermore, to accurately simulate the performance of our system in the ocean, no direct contact can occur with the system until its data collection has been completed (even in between sets of measurement). Thus, to retrieve the data it has collected, the sensory unit must be able to communicate wirelessly using an IEEE Standard compliant communication system (such as the recommended WiFi ESP8266 on the Huzzah).

1.3 Project Management

In order to meet the deadlines for operation and to pipeline the project in an efficient manner, a Gantt chart (updated weekly) was utilized as the primary organizational tool. This chart is displayed in Figure 18 in Appendix A.

1.4 Prototyping Costs and Bill of Materials

In this project, we were allocated an initial budget of \$200.00 to cover all necessary prototyping costs. To summarize, we estimate a final prototyping cost incurred of \$127.45 and a total expense of \$167.09, which includes back-up electronics and components ultimately unused in the final system. The precise list of components and their associated prices are given in B

The bill of materials is the cost of producing 10,000 units of our devices (utilizing bulk costs). The total bill of materials is \$989,015. For a complete cost breakdown, refer to Figure 20 in Appendix B

2 Theory of Sensor Operation

2.1 Colorimetry in Turbid Media

Our goal is to make optical colorimetry measurements to infer relative concentrations *independent* of the turbidity of the solution. A common configuration for this problem is shown in Figure 1. In this configuration, light from a source is incident on the sample and the transmitted light is received at photodetector PD1 on the other side. Because the intensity and spectrum received by PD1 is dependent on the absorption of the solution, one can infer the properties like the color of the solution from this photodetector's readings. For example, if the solution is pink (as in the case of Rhodamine WT), it *absorbs* wavelengths in the green region and *transmits* the red (and partially blue) wavelength regions¹. Thus,

¹ It should be noted that in this case, “pink” is *not* simply a case of “light red” but in fact is a combination of wavelengths in both extremities of the visible spectrum. This is reflected by Rhodamine’s absorption in the 500-600 nm wavelength region (green) and its low absorbance in the

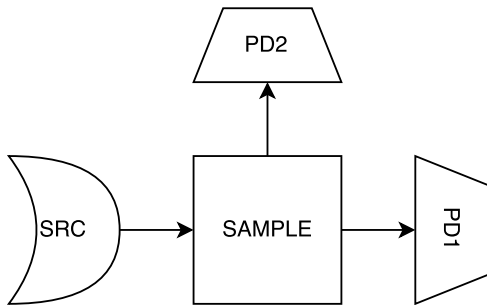


Figure 1: Schematic overview of a colorimetry technique for use in turbid media. The light source (SRC) is incident through the sample. Transmitted light is incident on the throughput photodetector (PD1) and scattered light is incident on the orthogonal photodetector (PD2).

the light received by the throughput photodetector will have an underrepresentation of the green wavelengths relative to the incident light. Furthermore, one can infer the concentration of dye in the solution by examining the *degree* of underrepresentation of the green wavelengths.

However, the turbidity of the solution can confound the results of an absorbance measurement. If the solution is very turbid, it will scatter some of the incident light in random directions, causing a decrease in the throughput received by PD1. Then, examining the raw absorbances of different wavelengths of light may lead one to falsely assume that the sample possesses a higher concentration of colored solution than it actually does. To correct for this problem, a second photodetector (PD2) may be placed orthogonally to the source and PD1. If the system is designed such that the source rays are not directly or indirectly incident upon PD2, then the light received by PD2 should be entirely due to scattering. One can then compare the amount of light received by PD2 and PD1 to infer the degree of turbidity of the solution.

It should be noted that this overall approach does simplify the optical phenomena that could confound the colorimetry measurements. First, this approach assumes that the photodetectors are not sensing any light other than that which was transmitted by the source. Thus, it is important to ensure outside light sources are blocked. Other issues which are not considered include the potential wavelength-dependence of scattering and its potential directionality. However, for the purposes of this design project, one may assume non-wavelength-dependent Lambertian scattering. Thus, this configuration and the aforementioned strategy is sufficient to perform colorimetry measurements.

Naturally, it is useful to develop a more quantitative approach to determining the concentrations of dye in turbid solutions. The general approach would be to establish a database

600-700 nm (red) and 400-500 nm (blue) wavelength regions. [4]

of calibration data from solutions of *known* concentrations and turbidities, and use some interpolation scheme to determine the concentration (and turbidity) of a new unknown solution. This strategy is discussed more thoroughly in Section 3.

2.2 Electrochemical pH Sensing

All pH sensors consist of three fundamental components:

1. A reference electrode.
2. A measuring electrode which is sensitive to hydrogen ions in solution.
3. An analog-to-digital (ADC) converter that converts the voltage difference between the measuring and reference electrodes into a digital pH measurement.

Specifically, the measuring electrode undergoes ion exchange with the solution, causing its relative charge (and thus voltage) to change. Because the amount of ion exchange that occurs is proportional to the pH of the solution, one can examine the relative voltage of the measuring and reference electrodes to determine the pH.

The electrochemical pH sensing model that will be used is based off of the design described in [5]. The premise of this configuration is that if two electrodes (metal rods) are submerged in a solution, they each undergo ion exchange, and the potential difference between those rods may be related to the pH of the solution. This is clearly the case if one metal is more electronegative than the other or attracts the hydrogen ions more strongly than the other. Of course, the precise relationship between the potential difference and pH may be quite complex depending on the material properties of rods, the distance between them, and their local environment in the solution. However, one can potentially map this relationship by collecting information from multiple electrodes. This is precisely the approach we take in our design project. We will be submerging three separate electrodes (titanium, stainless steel, and aluminum) referenced to a fourth zinc electrode for all measurements. Just as

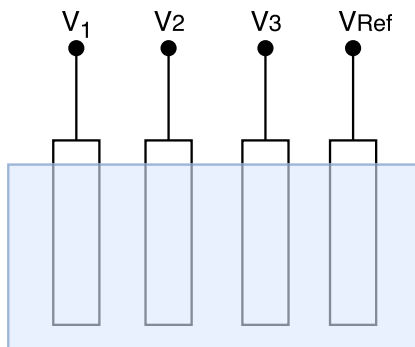


Figure 2: Schematic overview of the electrochemical pH sensing technique. Three submerged rods made of different metals each produce a voltage (V_1 , V_2 , and V_3) relative to the reference V_{Ref} .

with the colorimeter, the crucial step in determining the pH is calibration. Essentially, to determine the pH, one should take potential measurements in several solutions of known pH and attempt to build a model that can accurately map potential measurements to pH values. In doing this, it is also important to control for other factors that can influence potential measurements besides the pH of the solution, including the amount of surface area exposed and the distance between the rods.

3 Colorimetry

3.1 Capabilities

We've demonstrated that our colorimetry system can differentiate between concentrations at 5 ppm resolution, even in severely degraded samples as shown in Figure 3. Each data point corresponds to an average of $N = 100$, and three independent repeated measurements were performed for each concentration. The measurements are independent in that between each measurement the cuvette was removed, the entire system was re-set and put away, and at least 8 hours passed. We can even more easily distinguish different concentrations in fresh samples, as in the left panel of Figure 4 where we've shown that any color channel can be used to distinguish between concentrations at 10 ppm resolution. In addition, we've shown that our readings are remarkably stable over time if our system is protected from external light and forces. The *most* variable example from our fresh-sample testing is the color temperature data shown in the right panel of Figure 4. The fact that the readings were so stable over time and did not display much temporally fine-grained behavior has important implications for data collection. In particular, it means that we can obtain the essential features of the color data by sampling periodically over time.

3.2 Demo Day Data

We present our data from demo day in Figure 5. Clearly there is an increase in temporal variation, especially in the color temperature channel. We attribute this to the fact that color temperature is computed using all the other channels, so the combined small variations in each may have combined to substantially increase the variability of the color temperature. As noted previously, color temperature was the most variable channel even when all channels were remarkably stable. Furthermore, our previous stability and accuracy results were obtained in controlled conditions under which our sensor was not subject to external light or forces. During demo day testing, our colorimeter was subjected to vigorous agitation which may have affected our measurements. As is explained in later sections, the sensor geometry has actually not changed from our old testing environment to the new sensor – the same part was merely put in a new box. Thus, we do not believe this was a strong influence on our results.

4 Turbidity

4.1 Preliminary Testing

Preliminary testing for turbidity included examining the color channel readings for the photodetector orthogonal to the LED and determining whether these readings varied between solutions of different turbidities. We initially tested using solutions containing microspheres that had turbidities of 1, 3, 5, 7, and 10 NTUs. However, we found that the amount of light received by this orthogonal photodetector was dramatically lower than that of the throughput detector. For example, even with the highest turbidity solution (10 NTU), the maximum values for each color channel were 1-2 orders of magnitude smaller than the values obtained for the throughput detector during trials, as demonstrated in the table below. Thus, we determined that it was sufficient to ignore turbidity readings in our final demonstration.

4.2 Demo Day

The orthogonal photodetector readings for each channel are shown in the figure below.

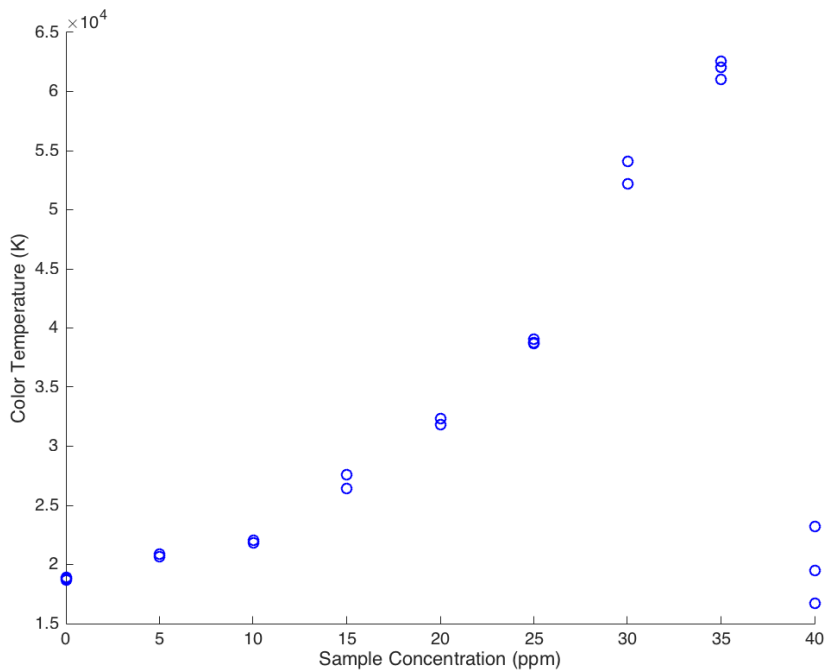


Figure 3: Distinguishability results at 5ppm resolution in degraded samples. Each data point is the average of $N = 100$ data points. The three points for each concentration correspond to repeated independent measurements over time. Note that error bars were deliberately excluded as they were in all cases very small relative to the intensity values – see Figure 4 for corroboration.

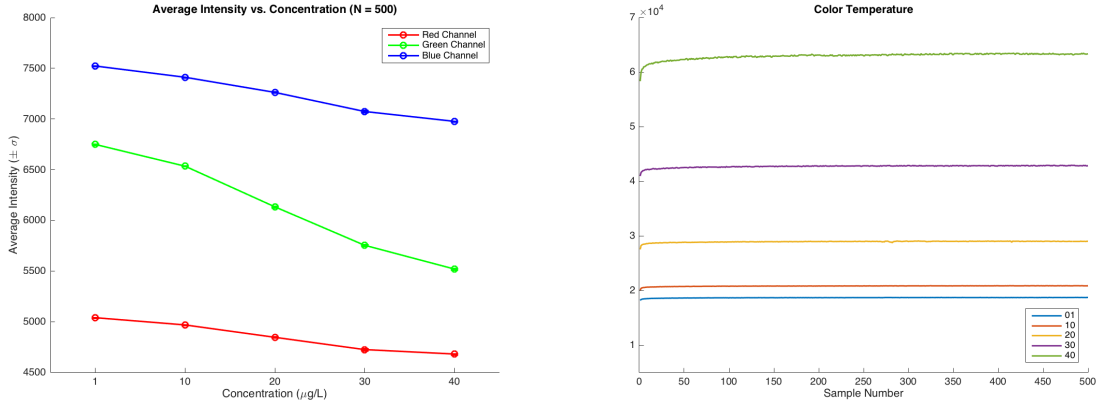


Figure 4: (Left) With fresh samples, any color channel can easily distinguish between concentrations at 10 ppm resolution. Each data point is the average of $N = 500$ data points. (Right) Even the most temporally variable channel from our fresh-sample testing shows remarkable stability.

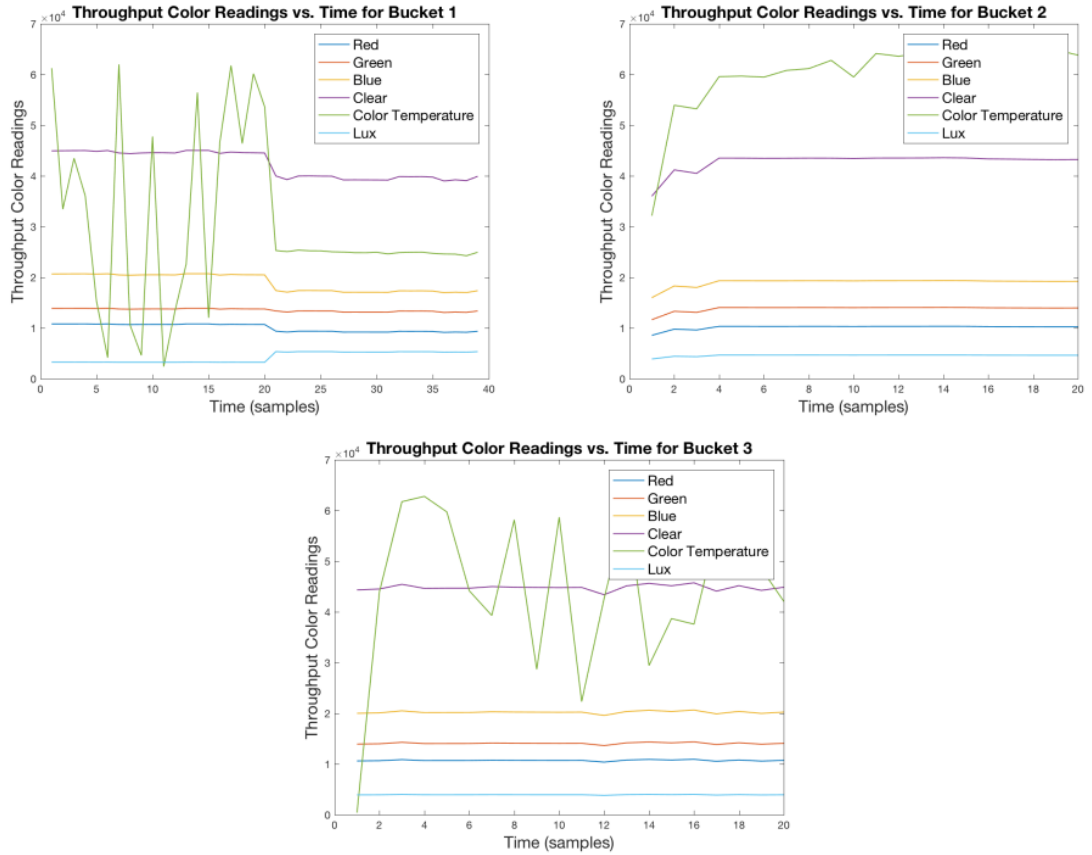


Figure 5: Colorimetry data from demo day testing.

	Red	Green	Blue	Clear
Transmitted	>5000	>6500	>7400	>19500
Scattered	<70	<130	<150	<400
Reduction Factor	71	50	49	49

Figure 6: Order of magnitude comparisons of scattering intensities to throughput intensities.

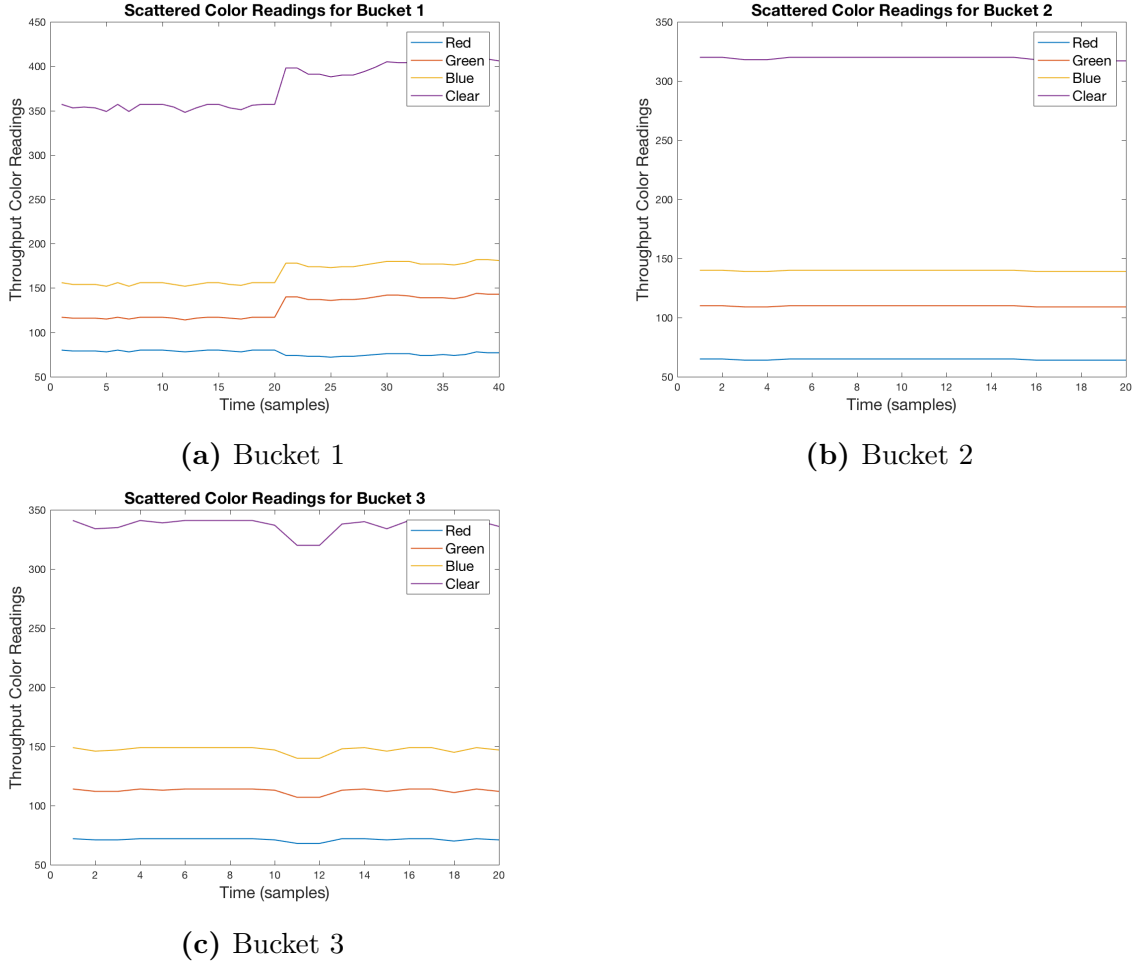


Figure 7: Transient Color Readings for Orthogonal Photodetector.

As one can see from the plots, the readings are relatively stable, and are all within the 50-400 value range. These readings were negligible compared to the readings for the throughput photodetector shown in Section 3, which are on the order of magnitude of 10^4 . Thus, the turbidity of the solution did not cause significant scattering, so the throughput photodetector readings can be taken at face value.

5 pH Sensing

5.1 Preliminary Results and Challenges

To determine the relationship between the voltage readings on the metal rods and the pH of the surrounding solution, we calibrated by using solutions of diluted HCl and NaOH. To mimic the chemical composition of oceanwater, the dilutions were prepared in 2:1 mixtures of DI water and instant ocean. When performing tests, in order to ensure that the voltage readings from each rod was an accurate representation of the amount of ions in solution, we made sure to sand and rinse the rods with DI water in between testing solutions of different pH's. This would remove the outer layer of the rod, which would have undergone ion exchange with the surrounding solution. To characterize the

settling times of the rods, we began by submerging the rods in solution and collecting 500 voltage readings over the span of about 7 minutes. The results indicated the rods required a 1-2 minute settling time to reach a stationary voltage, as shown in Figure 8.

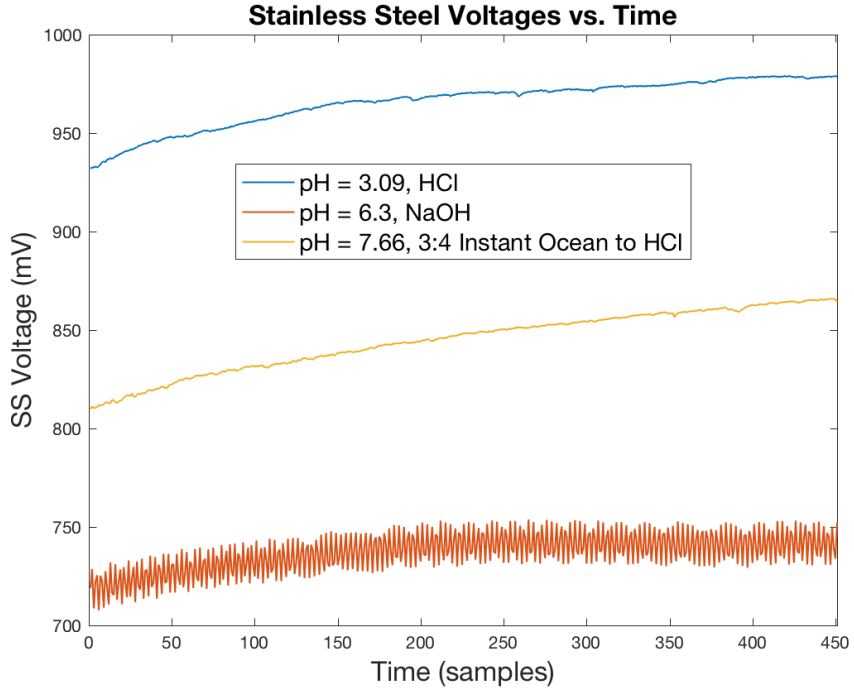


Figure 8: Time Dependence of voltage readings for stainless steel rod on three test solutions. The plot indicates that the rod needs some time for its voltage to begin to saturate at a final value. This final value was obtained by performing a nonlinear least-squares regression fit using a sigmoid function.

To obtain a representative voltage measurement for each solution that also accounted for this settling time, we performed a nonlinear least-squares regression fit using a sigmoid (s-curve) function. This function is a special case of the logistic function, and is commonly used for analyzing saturation behavior. The general expression for a sigmoid is as follows:

$$f(x) = A + \frac{K}{1 + e^{-bx}} \quad (1)$$

where A represents the vertical displacement of the sigmoid, K represents its asymptotic saturation value, and b represents the rate of incline towards the asymptotic value. Using this fit, we were able to read off the final voltages of each rod. The uncertainty in this value was taken to be the 95% confidence interval in the fitted parameter. An example for aluminum is shown in Figure 9.

Then plotting the final voltage against the known pH of the trial solutions would al-

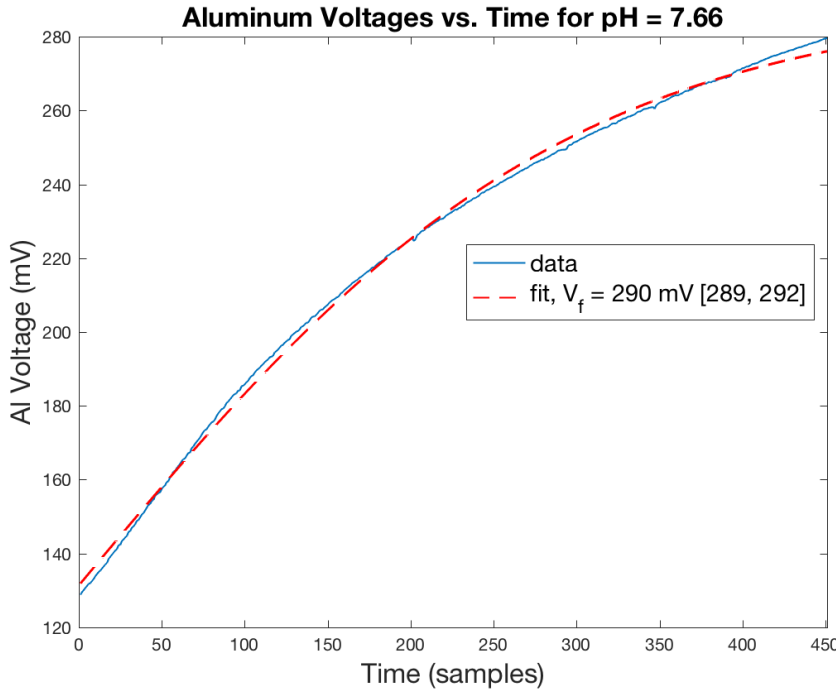


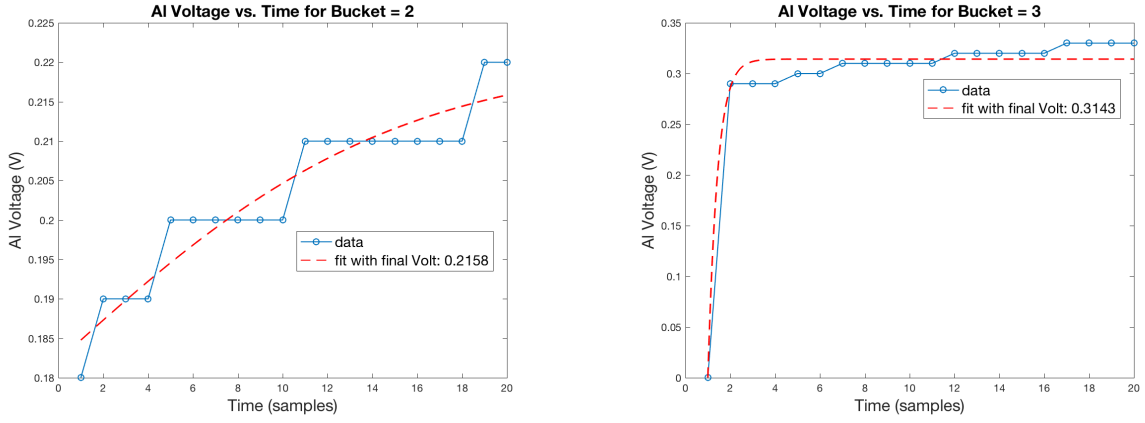
Figure 9: Example of a sigmoid fit of the voltage readings of the aluminum rod for a test solution. The asymptotic voltage V_f of the rod is shown in the legend, along with the 95% confidence interval bounds in brackets.

low us to calibrate our pH solution. We found that the voltage of the rods generally increased with the pH, but that the rate of increase was inconsistent between different trials. This can be attributed to some of the challenges we faced when performing the calibration. First, there was some difficulty in obtaining stable pH readings from the industry-standard pH meter, especially with the basic solutions. It was discovered that the NaOH solutions exhibited degradation over time, resulting in pH readings that were lower than expected. Furthermore, the breadth of the pH solutions that we had available were not representative of the span nor resolution of pH's that we were expected to be able to detect. Lastly, there was an apparent the lack of repeatability in the voltage readings such that for different trials of the same solutions, the rods obtained significantly different values. This indicated that while it is possible for our pH sensing subsystem to distinguish the *relative* pH's of unknown solutions, it would be much more difficult to obtain accurate absolute pH measurements of the unknown solutions.

5.2 Demo Day

The results from demo day indicated that our pH sensor is capable of distinguishing between solutions of different concentrations provided that it was in a stable configuration. For example, during one bucket trial, our system experienced significant shaking, which became evident in the transient voltage readings of the system. However, during a more stable trial, we were able to observe highly-stable transient readings. A comparison of

these two cases for the aluminum rod is shown in Figure 10.²



(a) Transient Readings for Aluminum for Bucket 2

(b) Transient Readings for Aluminum for Bucket 2

Figure 10: Comparison of the transient behavior for two bucket trials for the aluminum rod. The transient readings for bucket 2 shown in subfigure (a) are highly-unstable, continuing to climb in a stair-step fashion, whereas the readings shown for bucket 3 in subfigure (b) appeared to saturate at a final value. This discrepancy is likely due to shaking present in the system when testing with bucket 2.

For the sake of the final demonstration, we adopted the strategy of distinguishing between the *relative* pH's of the buckets. That is, we ranked the pH's of the buckets according to the final voltage readings on the rods. However, given more time to calibrate the pH sensor, we are reasonably confident that we would have been able to distinguish the absolute pH given the differences in the final voltages between the different buckets.

6 Final Design Prototype

In transitioning from the early theoretical work and the skill-set development mini-project which probed a basic implementation of colorimetric sensing, a final system design and casing was required. In addition to readily combining the electrochemical and colorimetric sensor into one unit, the final prototype at the end of the semester would also need to effectively hold all electrical components, facilitate wireless charging through one side of the device, enable stable waterproofing, and provide a quick turn-around for replacements or structural modifications. Here, we note that there were many options available for engineering the full system besides the one discussed in this work. Specifically, a system engineered from PVC pipes and related components instead proved to be not only largely popular but exclusively chosen by all present colleagues; however, we chose to proceed with engineering our system from 3D printed components. Here, we emphasize that the primary motivation for our design approach stems from the freedom and conveniences

² Only one example is shown below because it is representative of similar trends in the stainless steel and titanium rods between different bucket trials.

which 3D modeling and printing grants.

In this approach, our encasement can adapt and change to facilitate the necessary modifications in the sensor rather than having our sensors constrained to the dimensional and structural limitations of pre-built components. Furthermore, during the early prototyping stages, it was fully anticipated that unexpected issues may arise which would demand quick response and solutions in order to stay on track. In 3D printing all sensor encasements, the system could be re-printed and re-assembled in as little as half a day (excluding waterproofing treatments). Lastly, we highlight that the initial experimental testing for colorimetry was built upon a 3D printed assembly, and in proceeding further with this approach, we were ensured that our initial findings could be readily and easily adapted to the final product.

In the left image of Figure 11, we display the final prototype with the primary components labeled. To summarize our design, four conducting rods utilized for electrochemical sensing are attached to the primary housing at one end. On the other end, the two pins attaching the light screen to the box can be freely removed which then reveals the attached cuvette used for colorimetric sensing. This is displayed in the image on the right of the same figure. To provide a road map for the reader, in section 6.1 and 6.2, we review the specific details for each of these engineered sensor systems, followed by a discussion on the methodology utilized to waterproof the integrated, final design. In section 6.4, we then present a review of the potential environmental impact from our system, followed by a discussion of the challenges faced in developing our final prototype.

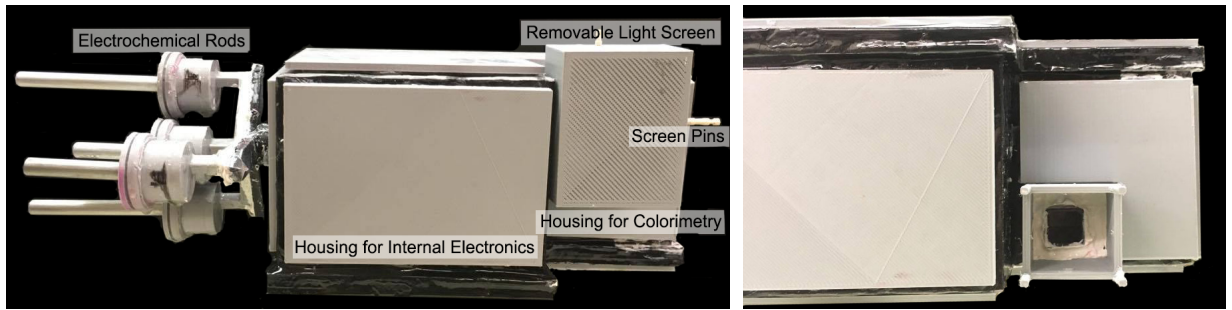


Figure 11: Overview of Final System Prototype: (Left) Photo of the integrated system design with primary components labeled. (Right) Photo of the housing for colorimetry with light screen removed.

6.1 Colorimetric Sensor Design

Operation of our colorimetric sensor, which is adapted to function in turbid liquids, utilizes two photodetectors and one LED arranged in the configuration shown in the left-most diagram of Figure 12 and outlined in detail in the theoretical review presented in section 2.1. Specifically, a photodetector and LED pair is arranged on opposite sides of the cuvette chamber and a second photodetector utilized for determination of scattering due

to turbidity is placed 90° relative to the other. A schematic of the cuvette chamber is shown in the middle diagram of Figure 12; however we note that this component is printed as a connected structure to the primary housing rather than as a separate piece in order to minimize the possible entry points for water. A cuvette is then inserted from the square hole at the top of the cuvette chamber/colorimetry housing and rests securely in place since the walls gradually become more narrow approaching the bottom. The cuvette has one end open (facing upwards) and is utilized as the interface which separates the detectors and the other electronics contained within the primary housing from the fluid. The three wide openings on the sides of the chamber are where the sensors are attached and operated.

For each photodetector and the LED, the electrical device is first attached to the corresponding fitted face-mounts shown in the rightmost diagram (labeled A and B, respectively). They do not require glue and are instead designed so that the devices can be pushed/clicked into place and held there by small, overhanging plastic ridges. These components were developed in order to provide a secure and stable method to position the electrical components on the cuvette chamber, and the grooves on one side of the mounts match the ridged tracks located along the columns. Once assembled, the face-mounts are lined up and glued into place. As a note, this is the exact assembly which was developed and tested in the skill-set mini-project and the similarity of the initial and final sensor design simplified the needed development for this sensor system. Although not observable in the preceding diagrams, the inside of the box was also coated with flat/matte black spray paint in order to minimize internal reflections.

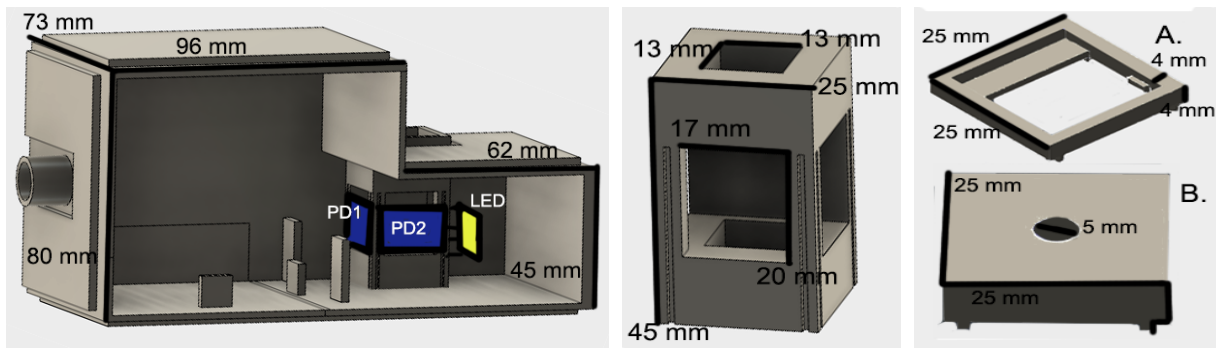


Figure 12: Schematic for the Colorimetry Sensor System. (Left) Diagram of the inside of the box where photodetectors, PD1 and PD2, mount (Middle) Diagram of the cuvette chamber. (Right) Diagram for photodetector and LED mounts

6.2 Electrochemical Sensor Design

In Figure 13, the final electrochemical sensor (left) and a schematic of the sensor encasement (right) is shown. In comparison to the colorimetric sensor, the design considerations are somewhat simplified due to the reduction in overhead electronics. Specifically, the utilized design was entirely motivated by considerations for the stability of the rod and the ease in transitioning to waterproofing and final integration to the primary housing. A discussion

of the assembly methodology for this sensor system is presently deferred to subsection 6.3; however, we note that this component was fully assembled separate to the colorimetry sensor system and the primary housing, thus allowing full testing and usage prior to any waterproofing treatment or connections to the main assembly. For this reason, all four metal rods—stainless steel, titanium, zinc, and aluminum—were integrated into the design with determination of their usability in sensing ocean water to be tested at a later time.

As should be noted from the right diagram of Figure 13, the geometry utilized is not arbitrary. The center cylindrical case housing the zinc rod is positioned at an equal distance from each of the outer three rods. This was motivated by the fact that each outer rod measures a potential difference relative to the zinc rod located at the center, and to facilitate the early analysis for the difference in sensing between the different metals, it was necessary to keep the spacing consistent. Furthermore, to minimize the possibility of cross-talk between the outer rods, the angle between each was designed to be 180° thus maximizing the separation distance. A wire is connected to each rod by a metal clamp concealed inside each individual, cylindrical rod holder and the wiring runs through the hollow tubing and into the primary housing.

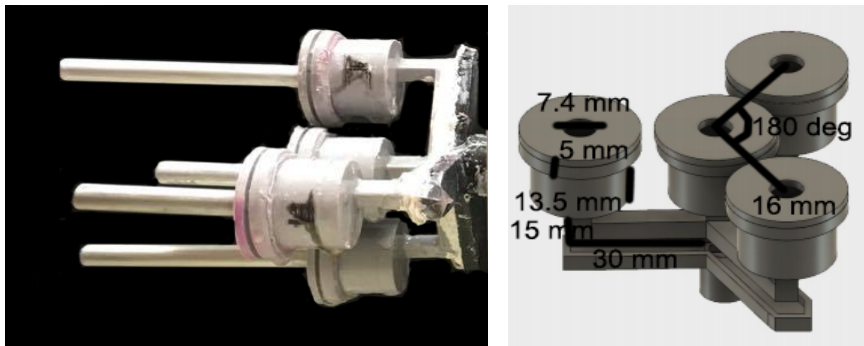


Figure 13: Photo of the Electrochemical Sensor which is connected to the final, primary housing

6.3 Waterproofing

One of the primary concerns with 3D printing the encasement for our sensor system was the potential challenges associated with waterproofing. Despite this fact, after applying one full treatment to the final prototype, we found the system to be completely sealed and functioning for use in a marine environment with no unexpected challenges or difficulties faced. To summarize our methodology for this, we first begin by identifying what we believe to be the three primary regions of compromise at which water could penetrate the encasement.

- At the electrochemical-primary housing connection depicted in the left-most diagram of Figure 14,
- the cuvette-primary housing connection depicted in the middle diagram,

- and the lid-primary housing connection depicted in the right-most diagram.

Here, we summarize our solutions to each of these areas; however, we first note that the PLA plastic utilized for 3D printing is porous. Although initial testing conducted on a 3D printed box with a wall thickness of 1 cm showed no water leakage after filled with water and allowed to rest for two hours, our final prototype with a wall thickness of 2.5 mm would not be effective in blocking out water. To counter this issue, all 3D printed walls were given one coating of marine epoxy on its outer face, and this treatment proved to be more than sufficient. Before proceeding to the main waterproofing methods, we also note that an initial layer of highly viscous superglue was applied to all junctions in which marine epoxy or marine sealant were to be applied. This allowed better containment of the epoxy as well as sealing fine joints and imperfections which cannot be easily reached by the thicker medium. Complete and effective waterproofing was determined by placing paper-towels along the inside of the box and partially submerging the enclosure under water for 1 hour. After the time had elapsed, the towels inside the box were inspected. For all system tests, no water was observed.

First, in addressing the waterproofing treatment for the electrochemical-primary housing connection, we note that the electrochemical sensor system, excluding the rods, contains three separate components—the cylindrical cups, the fitted cup lids, and the joint-tubing lid—these all can be observed by examining 1a. in the leftmost diagram of 14. The rods which are clamped to the wires and placed inside the cylindrical shape holders. These cups are then individually filled with marine epoxy and the lids, which have a ridge fitted to the groove on the top of the cup, are combined and thus sealed. At this point, the connection between the wire and the rod is secured. From there, the wires run through the hollow tube which connects all four individual cups and this tubing is then filled with marine glue. The matching shaped cover for this tube can be seen from the diagram, and we highlight that it has a cylindrical tube on its end with an outer radius slightly smaller than the inner radius of the cylindrical tube protruding from the primary housing. The two are joined at this interface and after the wires are pulled through into the box, the cylindrical tube is then filled with marine glue thus ensuring a waterproof system and connection.

For the cuvette-primary housing connection, we previously noted that the cuvette is placed into the cuvette chamber from the square hole at the top which is qualitatively depicted in the middle diagram of Figure 12. As can be observed in 2a. of Figure 14, this placement results in the open end of the cuvette protruding from the face of the primary housing by approximately 5 mm. This elevated region then underlies our fundamental method for waterproofing used here. Shown in the same diagram, a rim 5 mm tall is glued to the face of the box and the region in between, denoted with the white lines, is filled with a pool of

marine glue which forms a bond to the cuvette's protruding walls. This then results in a quick and efficient method for ensuring no water could enter at that junction.

Lastly, we note that, as seen in the left-most diagram of 12, the primary housing has one open wall which is required to insert all the electronics and circuitry. To seal this once the internal components are placed, the lid diagrammed in 3a. of Figure 14 was utilized. We note that the lid with a rimmed edge is slightly larger in dimensions than the open face of the box (with the contours being otherwise the same). The lid is then filled with a pool of epoxy in the region denoted with the white striped lines and the primary housing is then inverted and placed firmly against the lid. The pool of epoxy which bonds to both the inside and outside of the submerged primary housing walls thus ensures a water-tight seal.

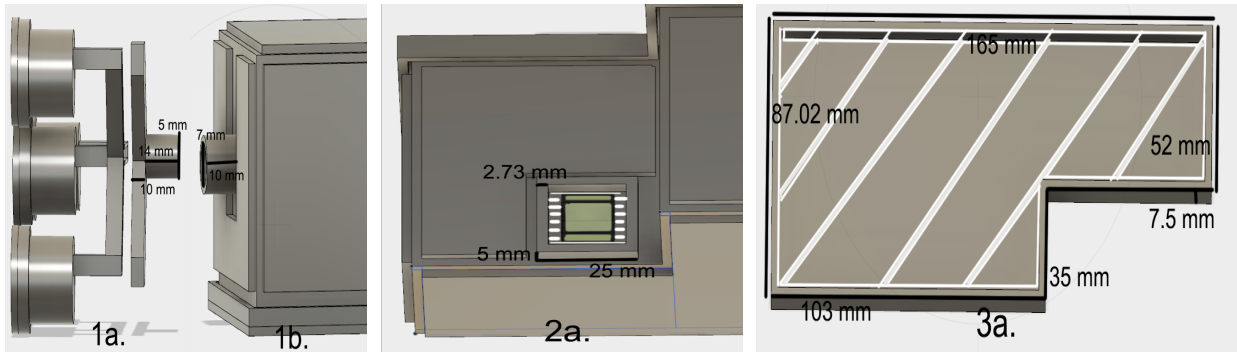


Figure 14: Diagram for the three main points in the system design where additional waterproofing treatment was needed. White Lines indicate where marine sealant was utilized. (Left) Figure 1. electrochemical-primary housing junction. (Middle) Figure 2. cuvette-cuvette chamber junction. (Right) Lid-primary housing junction.

6.4 Environmental Impact

In evaluating the environmental impact of our proposed system, we first briefly review the potential risks to the marine environment (or the larger environment if applicable) associated with each material utilized here—PLA or ABS plastic from the 3D printed casing, marine glue/marine epoxy, the metallic rods, and the grouping of additional internal electronics and components. For anticipated operation in the ocean environment, the system only requires brief submersion for data analysis, and thus we will presently ignore the scenario of the system lost at sea. In all cases, it should be readily retrievable or connected to the surface/operator and can thus be pulled up from submersion by rope. For this reason, we then ignore the potential risks associated to the metallic rods and the internal components, instead focusing on the risks of the epoxy and the plastic.

First, we note that from research conducted and published by SP Systems, one of the leading manufacturers of marine epoxy, the primary environmental risks associated to the use of laminates stems from the potential water degradation of the mixture. All epoxies and resins will absorb moisture when submerged for extended periods of time; however, the associated risks depend largely on how the absorbed water affects the

mechanical properties. Both polyester and vinyl resins have been found to be prone to water degradation due to the hydrolysable ester group in their chemical structure, and after submersion over a period of one-year, research suggests that a thin polyester laminate can be expected to lose approximately 35% of its inter-laminar shear strength. General epoxies, alternatively, have been found to lose only around 10% over the same period of time with various companies specifying different values for their mixture of marine epoxy [15]. Furthermore, if we examine the potential usage of a marine-brand epoxy like that sold from West Systems, we can begin to quantify the associated risk. It is common for emission standards to identify the emission or pollution potential for a compound via approximation of the amount of volatile organic compounds (VOCs) which will be emitted. Citing values published by West Systems, 100 L of conventional vinyl ester resin would be anticipated to release approximately 12 Kg of VOCs into the air, while the same amount of their marine brand epoxy is cited to emit only around 454 g of VOCs—well within the limits set by emission standards and suggested to be near the potential upper bound for the true VOC count of epoxies cited to contain 0% VOCs. Furthermore, we note that according to US standards, hardened epoxy is defined to be a non-hazardous solids presenting little risk to the environment [16].

In addition to the usage of marine epoxy, our system is predominantly comprised of 3D printed plastic—most commonly either PLA or ABS plastic—and here, we briefly comment on the potential risks for both scenarios. Polylactic acid (PLA) is a plastic substitute made from fermented plant starch, typically corn. As a result, this form of plastic is entirely organic and fully biodegradable and does not pose significant environmental risks directly. Presently it is unclear if there exists indirect consequences, but for the amount of plastic required by our system, we assume that most postulated, indirect risks will prove negligible [17]. In regard to ABS plastic, recent studies have suggested the potential that chemical degradation, particularly when exposed to high temperatures, may result in the emission of toxic particles [18]. To err on the side of caution, our system should be sufficient if manufactured from PLA rather ABS since structural support can be ensured in alternative ways. Our final conclusion is that we find there are very limited environmental risks presented by our proposed system.

6.5 Comments on Design Challenges

The primary design challenge experienced while engineering this system resulted from a slight oversight in ensuring that the box would sink when placed in the ocean water. Specifically, upon running a full system test, it was discovered that our current box floats unless additional force or weight is added. In the initial proposed design, we had planned to fill the entire box with epoxy, but since that early stage, we had instead chosen to bypass that option to allow for greater flexibility and access to the internal components. A baseline calculation was conducted for the system where we approximated the volume of

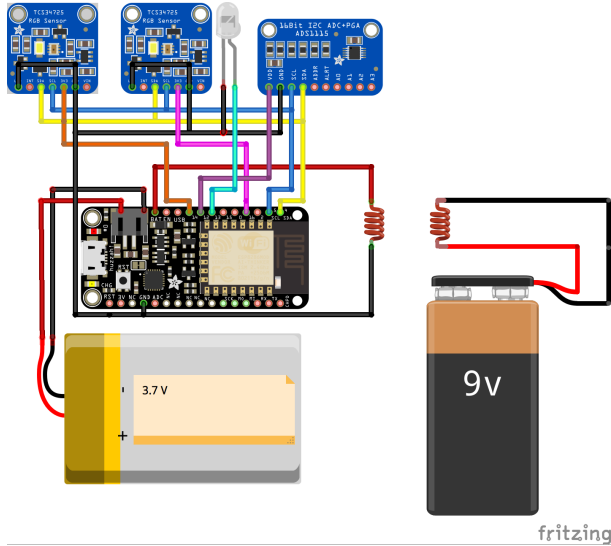


Figure 15: Final electronics design.

the air enclosed in the box to be 764.310 cm^{-3} . For water with a density of $1\text{g}/\text{cm}^3$, this volume then implies that 764.310g of water is displaced thus resulting in a buoyant force requiring ≈ 1.7 lbs to counteract. Although the system itself was not rigorously weighted, we had believed that the box had exceeded this weight but further testing is required.

7 Electronics and Power

In this section, we describe the design of our electronics, estimate power consumption and battery life, and discuss related challenges.

7.1 Electronics Assembly and Design

We provide a Fritzing diagram of our final electronics design in Figure 15. The Feather is powered by a 3.7 V 6600 mAh lithium ion battery. The battery is connected to an inductive charging coil which has an external counterpart connected to a power source for charging. Our electrochemical sensing electrodes (not shown) are connected to the ADS1115 analog-to-digital converter (ADC) – three to input pins and one to ground. We also have two TCS34725 color sensors for dye concentration sensing and turbidity sensing. The color sensors and the ADC all communicate with the Feather using the two-wire I²C protocol. Finally, we have a clear LED for illuminating our water sample for color sensing. The LED, ADC, and color sensors are all powered by digital output pins, which allows us to manage power consumption and address conflicts. In particular, the two color sensors both have the same immutable I²C address so they cannot be on simultaneously. All delicate connections were reinforced with hot glue and coated with heat shrink for strain relief. For the color sensors in particular, we were able to run one fewer wire back to the Feather by soldering the LED pin directly to ground. This modification and our strain relief solution can be seen in Figure 16.

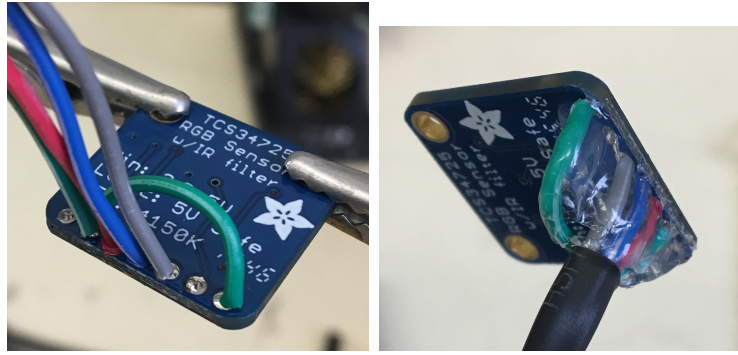


Figure 16: Solder joint reinforcement and strain relief.

7.2 SD Shield

We were never able to reliably store more than about 30 complete measurements (consisting of red, green, blue, clear, lux, color temperature, and three ADC voltage channels) on the Arduino. To be safe, we would actually need to stay closer to 20. This led us to purchase an Adalogger FeatherWing [12] and an 8 GB SD card to provide a vast reserve of flash memory for our sensor. We were able to demonstrate perfect read and write functionality when using the FeatherWing in isolation, but when we attempted to integrate it with the full system the color sensors began to malfunction. In particular, the problem was triggered by executing the command `SD.begin()` which initializes the SD card and the SD library. [13] Given that we were short on time, we decided not to utilize the FeatherWing's capabilities in our final sensor (though we did include the hardware). Only being able to perform 20 or so measurements is not quite as restrictive as it sounds. Since we were not interested in fine-grained temporal behavior of either pH or dye concentration, collecting intermittent samples spread out over time actually makes a lot of sense. In addition, it allows us to conserve power by turning on the sensors and LED less frequently.

7.3 Inductive Charging

Wireless charging capabilities were essential for sensor reusability due to our sealed-case design. We used an inexpensive commercial inductive charging set composed of a transmitter coil, a receiver coil, and affiliated circuitry for each. [10] Per the documentation, we expect a 5 V supply at the output with about 40% energy transmission efficiency. When installed in our enclosure and tested, we initially observed a stable current draw of approximately 140 mA at 11 V DC for a transmitted power of $40\% \times (140 \text{ mA}) \times (11 \text{ V}) = 0.616 \text{ W}$ and a corresponding regulator input current of $(0.616 \text{ W})/(5 \text{ V}) = 123.2 \text{ mA}$. If we assume all of this current was used to charge the battery with perfect efficiency, we can compute the ideal full-charge time to be $(6600 \text{ mA/h})/(123.2 \text{ mA}) \approx 53.6 \text{ h}$. Obviously faster charging would be desirable. Both coils are air-core transformers, which are notoriously inefficient. [14] In an attempt to increase charging speed, we added a standard U.S. nickel (75% Cu, 25% Ni) in the plane of the transmission coil to approximate a solid-core transformer. This increased the stable current draw to 220 mA at 11 V DC,

which increased our transmitted power to $40\% \times (220 \text{ mA}) \times (11 \text{ V}) = 0.968 \text{ W}$ with a corresponding regulator input current of $(0.968 \text{ W})/(5 \text{ V}) = 193.6 \text{ mA}$ and an ideal full-charge time of $(6600 \text{ mA/h})/(193.6 \text{ mA}) \approx 34.1 \text{ h}$. This is starting to become a reasonable amount of time, and we could likely decrease it further by also adding a metal core to the receiver coil and by decreasing the thickness of the wall separating the two coils. However, it's not clear that we'd want to increase the charging rate any further because of the troubling amount of heat generated by even the lowest current configuration. Charging for just 3-5 hours (with the metal core acceleration) caused enough heat to start to melt the 3D printed wall. Charging overnight with no supervision would almost certainly be dangerous.

7.4 Battery Life Estimation

For all calculations in this section, we assume an *ideal* 6600 mAh battery capable of 100% charge and discharge. First, let's calculate an upper bound on battery life. If we were only powering the ESP8266 in its lowest current active state (60 mA) and assumed all other current draws were negligible then we'd have $(6600 \text{ mAh}) / (60 \text{ mA}) = 110 \text{ hours}$ of battery life. The Feather documentation recommends leaving a conservative 250 mA for the onboard electronics and the ESP8266. Each digital pin on the Feather is rated for 12 mA maximum current draw, so we can add in constant maximum draws for each of the four devices we're powering with digital pins to get a lower bound of $(6600 \text{ mAh}) / (298 \text{ mA}) \approx 16.58 \text{ hours}$. Of course, the four devices are not on all the time so we expect battery life to be a bit higher than this lower bound in practice. In addition, 250 mA is a conservative peak-draw rating for the ESP8266 and associated electronics, so that's certainly an over-estimate as well.

8 Wireless Communication and Data Management

8.1 Motivation

To provide a simple, reliable, and automated means of storing and analyzing experiment data, and to allow design of a fully closed system, it is necessary for the device to communicate collected data wirelessly. With such a communication protocol in place, the system can more easily be waterproofed, as serial communication is no longer necessary.

8.2 Overview of Communication Model

8.2.1 Client-Server-Database Model

Our communication protocol follows the client-server communication model. In this model, there are two primary "entities" – clients, and server(s). The server presents an API with which it can be communicated with, and clients communicate with this API. Since clients and the server are on different devices, this communication is handled by the HTTP protocol. In the simplest form of this protocol, clients send GET requests to a HTTP endpoint to request a specific resource, and POST requests to add an item to a specific

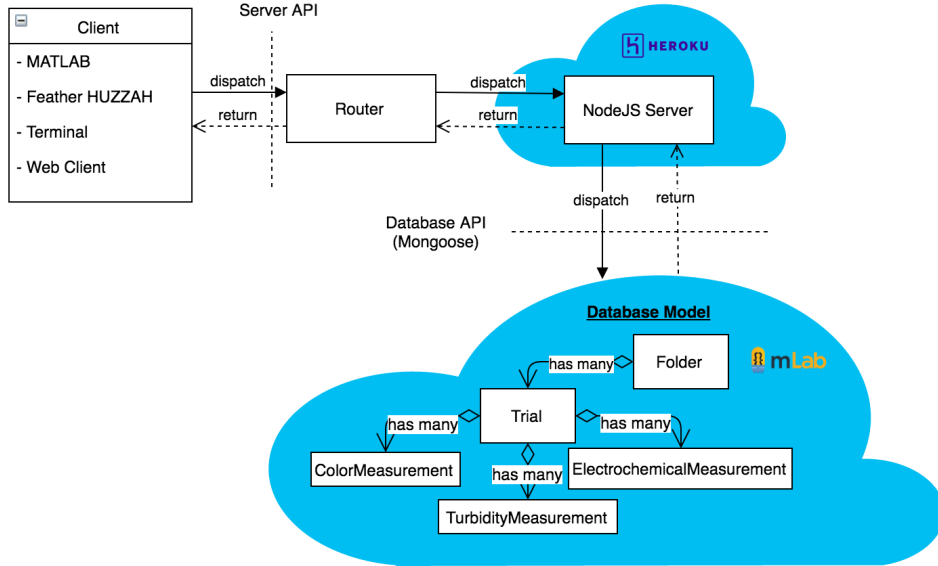


Figure 17: Outline of client/server/database wireless communication model

resource. Though there are more request types that can be made over HTTP protocol (for example, DELETE requests), none of these were necessary for this project.

8.2.2 Server

The server was written using JavaScript and the ExpressJS framework. In order to ensure the server was always live and available, the Heroku hosting platform was used to remotely deploy our server, and to provide a domain name to access the website. Heroku provides hosting of one *dyno* (essentially a black box that can be treated as a single server) for free. Since our simple application only required a single server, the free tier suited our purposes.

An alternative to remotely hosting the server is starting the server locally on one of our laptops. While this alternative would have avoided using an additional service, it would have required an additional step of starting the server every time we wanted to run an experiment. Since Heroku's service is free and easy to use, we see our choice to host the server remotely as the superior alternative.

It should be noted that, if Heroku's service were to go down, we could easily start the server locally. Thus, the choice to use Heroku is solely for convenience of access.

8.2.3 Database

The team chose to use a non-relational Mongo database hosted by a remote service called mLab [19]. We chose to use a non-relational database because (1) the team was more familiar with this service than relational database services, (2) Mongo databases structure their documents like JSON objects, so reads from and writes to the database were very simple, (3) mLab offers 0.5 GB of free storage, and (4) mLab offers an easy-to-use database management service through their website, which simplified data management.

The team viewed using a remote database (as opposed to setting up the database on the same machine as the server) as the simplest choice for using a database. Using a remote service made setting up the database quite simple, as mLab managed all setup and server allocation. Using a remote service also allowed us to use the same database during development on the local machine as was used by the server launched on Heroku. This meant less setup was necessary.

The main downside to using a remote database is the risk of the service going down and losing access to our data. While we did not experience this issue, it could have hindered our progress if it did happen. In order to avoid this issue, we could have instead used a local database such as SQLite [20]. However, this solution would have forced our team to host the server from a local machine, since Heroku servers do not support using SQLite. The best solution to this problem would be introducing redundancy to our database, either by purchasing additional database provisions through mLab, or by using multiple database services. For simplicity, our team chose to use only the free tier of mLab's services.

8.2.4 Router

In order to issue HTTP requests, clients must be connected to a wireless network. The TP-Link N300 router provides a private wireless network to which clients can connect and transmit data through the HTTP protocol.

8.2.5 Clients

Due to the incredible flexibility that the HTTP protocol provides, a client is any device that can issue HTTP requests. Thus, many clients are able to communicate with the server.

MATLAB

HTTP requests can be issued in MATLAB using the `webread` command. Using this command, experiment data can be easily obtained from the database for data processing and analysis on any computer immediately after the data is saved to the database. With a MATLAB data analysis script set up, one can generate analysis plots immediately after the experiment completes.

Feather HUZZAH

HTTP requests can be issued by the Feather HUZZAH by using the `ESP8266HTTPClient` library. However, since the request bodies and the response data are most easily constructed and parsed using JSON, the `aJson` Arduino library [21] was also used to simplify HTTP request construction and response parsing.

Terminal

The terminal client can issue HTTP requests through the `curl` command. This client proved incredibly valuable in debugging server functionality. By using `curl`, one can construct GET and POST requests to quickly check that the server API functions as expected.

Web Client

The web client is a website written using **React** [22] view library for presentational components, **Bootstrap** [23] for styling, and **Redux** [24] for overall application structuring. The website is served by the sever described in Section 8.2.2, and can be accessed via a domain name provided by the Heroku [25] service.

See Appendix C for how to access the website, as well as photos of the website.

Although all functionality of the website could have been replicated using only the terminal, the website presented an easy-to-use interface for initiating experiments, monitoring experiment progress, and organizing data from experiments. Since the website can be accessed on a computer or on a smartphone, any member of the team could initiate experiments from anywhere. Since the website was custom, the team was able to modify the site to suit our needs as new features became necessary.

8.3 Experiment Initiation, Monitoring, and Organization

Experiments are initiated on the website shown in Appendix C. To start an experiment, one can specify the turbidity, concentration, and pH settings of the experiment (note that, although the pH field is not currently displayed on the website, one can easily specify the pH by entering the information either in the turbidity or in the concentration fields, by using the convention CONCENTRATION_pH_PHVAL). One may also specify the number of measurements to take, the amount of time (in milliseconds) to wait before taking measurements, and the amount of time (in milliseconds) to take measurements.

Once this information is entered, pressing the **Run Experiment** button gives the "ready" signal to listening devices (the Feather) to begin taking measurements. Once the Feather receives this signal, the **Last time was alive** field on the website will update. This is the signal to place the device under water to begin taking measurements.

Once the measurement collection has completed, and once the Feather reconnects to the router, the measurements will be saved to the database and push notifications will be sent to the **Experiment Status** section of the website.

All trials (series of measurements) are displayed on the **Trial Data** section of the website. One can group these trials together into Folders using the **Folder** page on the website.

8.4 Troubleshooting

8.4.1 Reliable data transfer

Ensuring that the data was reliably saved was trickier than expected. Our code was initially written assuming that the Feather would always be connected to the router. However, when the device is submerged in water, wireless communication using the standard 2.4GHz is not feasible for appreciable distances larger than 10 cm[6, 7]. To resolve this issue, we

created a measurement queue in the Feather code to store the measurements until the device reconnects to the router.

8.4.2 Memory limits

The solution solved the connection-loss problem posed in the previous section created another problem with onboard memory capacity. We found that we could only reliably store 90 measurements (30 of color, turbidity, and electrochemical) on our device before memory limits were reached. In an effort to remedy this issue, we attempted to use external memory with an SD card. However, as discussed in Section 7.2, this solution produced more issues. Thus, we avoided the memory limits by limiting the number of measurements taken on the device.

8.4.3 After closing the case

Our case design introduced an interesting challenge to wireless communication – after our case was fully waterproofed, the case could not be taken apart. Thus, modifying the code uploaded to the Feather was not possible. As a result, we introduced several features to allow as much flexibility in our code as possible after it was updated.

1. **Dynamically configurable delays.** When requesting a new experiment on the website, one can specify the amount of time the Arduino should delay *before* taking measurements and *between* measurements
2. **Constantly waiting for an experiment.** Since we could not simply reset the device, the device constantly waits for a start signal from the server. After completing a requested series of measurements, the device goes back into waiting mode until it receives another signal.
3. **Alerts for device communication.** After the device was sealed, we no longer were able to verify that the device was taking measurements based on a LED signal. Thus, we introduced a field on the website that indicated the last time that the device had initiated communication with the website. This allowed us to know when the device was ready to be submerged in water.

9 Conclusions

In this project, we present a fully built and operational prototype for the colorimetric and pH sensing applications specified by the Ocean XPRIZE challenge. The final casing and system design is manufactured entirely from 3D printed PLA plastic and presents a single-unit cost of \$127.45, competitively priced among competitors. Furthermore, we have analyzed the potential risks and determined that there are no serious adverse environmental impacts from the systems long and short-term usage. To summarize the work done in this project, our final system design couples a four-rod electrochemical sensor to determine pH with a dual photodetector-LED pair to determine color in a turbid

liquid. The system has a fully integrated wireless charger and is set-up to connect and communicate over the internet with data storage and the primary interface hosted on the cloud.

A Gantt Charts

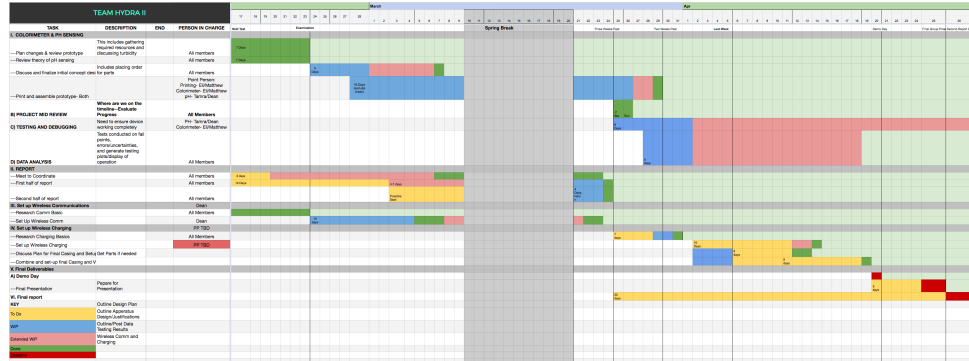


Figure 18: Gantt Chart

B List of Expenses

Item	Quantity	Unit Price	Total Cost
initial cuvettes	5	\$0.18	\$0.92
new cuvettes	200	\$0.13	\$25.80
color sensor	3	\$12.95	\$38.85
clamps	4	\$3.25	\$13.00
Adalogger FeatherWing SD Add On	1	\$13.99	\$13.99
8GB SD Card	2	\$5.99	\$11.98
LED's	1	\$0.95	\$0.95
Feather microcontroller	2	\$16.95	\$33.90
16-Bit ADC	1	\$14.95	\$14.95
Heroku Server Hosting Free Tier	1	\$0	\$0
mLab Database Free Tier (0.5 GB)	1	\$0.00	\$0.00
All 3D printed components	212.5 g	\$0.06/g	\$12.75
PROTOTYPING COST			\$127.45
TOTAL COST			\$167.09

Figure 19: List of Costs– Total Expenses during prototyping phase

Item	Quantity for one device	Unit cost	Total Cost
cuvette	1	\$0.13	\$0.13
color sensor	2	\$6.36	\$12.72
Feather microcontroller	1	\$13.56	\$13.56
16-Bit ADC	1	\$11.96	\$11.96
Aluminum rod	1	\$0.29	\$0.29
Stainless Steel Rod	1	\$0.15	\$0.15
Zinc Rod	1	\$0.50	\$0.50
Titanium rod	1	\$0.39	\$0.39
Ring clamp	4	\$3.25	\$13.00
protoboard	1	\$3.60	\$3.60
Inductive charging set	1	\$7.96	\$7.96
3.7V Lithium Ion battery	1	\$23.60	\$23.60
Epoxy (in oz)	6	\$0.44	\$2.64
Marine Sealant (in oz)	1.5	\$1.70	\$2.55
White LED	1	\$0.70	\$0.70
100 ohm resistor	1	\$0.50	\$0.50
PLA plastic (in grams)	240.5	\$0.02	\$3.61
Hot glue stick	0.1	\$0.44	\$0.04
Solder + wire (upper bound estimate)	1	\$1.00	\$1.00
		Total Cost for 1 device	\$98.90
		Bill of Materials (produce 10,000)	\$989,015.00

Figure 20: Bill of Materials calculated for production of 10,000 Units

C Documentation and Links

Our code may be accessed on our Github:

<https://github.com/tamran/Team-Hydra-II>

The Arduino code uploaded to our Feather Huzzah is in the **featherWifiCode** folder, the client-side code for the website is in **src** folder, and the server code is in the **server** folder. The MATLAB code can be found in the **matlab scripts** folder.

The website with our database of trial data may be accessed here:

<https://team-hydra-ii.herokuapp.com/>

A picture of the site is included in Figure 21

Figure 21: The four pages of our website

References

- [1] "Overview", Shell Ocean Discovery XPRIZE, 2017. [Online]. Available: <http://oceandiscovery.xprize.org/about/overview>.
- [2] A. Industries, "ADS1115 16-Bit ADC - 4 Channel with Programmable Gain Amplifier ID: 1085 - \$14.95 : Adafruit Industries, Unique & fun DIY electronics and kits", Adafruit.com, 2017. [Online]. Available: <https://www.adafruit.com/product/1085>.
- [3] Overview | Adafruit Feather HUZZAH ESP8266 | Adafruit Learning System", Learn.adafruit.com, 2017. [Online]. Available: <https://learn.adafruit.com/adafruit-feather-huzzah-esp8266/overview>.
- [4] A. Earp, C. Hanson, P. Ralph, V. Brando, S. Allen, M. Baird, L. Clementson, P. Daniel, A. Dekker, P. Fearn, J. Parslow, P. Strutton, P. Thompson, M. Underwood, S. Weeks and M. Doblin, "Review of fluorescent standards for calibration of in situ fluorometers: Recommendations applied in coastal and ocean observing programs", Optics Express, vol. 19, no. 27, p. 26768, 2011.
- [5] M. Brooke et al., "An ocean sensor for measuring the seawater electrochemical response of 8 metals referenced to zinc, for determining ocean pH.," *2015 9th International Conference on Sensing Technology (ICST)*, Auckland, 2015, pp. 147-150.
- [6] C. Xianhui et al., "Re-evaluation of RF electromagnetic communication in underwater sensor networks." *IEEE Communications Magazine* 48.12, 2010, pp. 143-51.
- [7] N.W. Bergmann et al., "Wireless underwater power and data transfer." *38th Annual IEEE Conference on Local Computer Networks - Workshops* , 2013.
- [8] "TCS3472 COLOR LIGHT-TO-DIGITAL CONVERTER with IR FILTER." TCS3472 Data Sheet. Web. <<https://cdn-shop.adafruit.com/datasheets/TCS34725.pdf>>.
- [9] Mixture, H. Chips and R. Accelerator, "Instant Ocean. At Home in America's Largest Aquariums.", Instantocean.com, 2017. [Online]. Available: <http://www.instantocean.com/>. [Accessed: 26- Apr- 2017].
- [10] "Inductive Charging Set - 5V @ 500mA max," Adafruit Industries, 2017. [Online]. Available: <https://www.adafruit.com/product/1407>.
- [11] "ESP8266 specification sheet," Adafruit Industries, 2017. [Online]. Available: https://cdn-shop.adafruit.com/datasheets/ESP8266_Specifications_English.pdf.

- [12] "Adalogger FeatherWing - RTC + SD Add-on For All Feather Boards," Adafruit Industries, 2017. [Online]. Available: <https://www.adafruit.com/product/2922>.
- [13] "Adafruit SD Library," Adafruit Industries, 2017. [Online]. Available: <https://github.com/adafruit/SD>.
- [14] M. E. Brumbach, *Industrial Electricity*, 8th ed. Clifton Park, NY: Delmar Cengage Learning, 2010. pp. 201.
- [15] "Environmental Issues," West Sys.,
<<http://www.westsysteminternational.com/en/support/environmental-issues>>. UK
- [16] "The Advantages of
Epoxy Resin versus Polyester in Marine Composite Structures". SP Sys., Newport, UK.
<<https://www.mjmyachts.com/images/stories/pdf/sp%20advantages%20of%20epoxy%20resin.pdf>> 2016
- [17] "The Environmental Impact of Corn-Based Plastics," Scientific American.
<<https://www.scientificamerican.com/article/environmental-impact-of-corn-based-plastics/>>
- [18] "3D Printers Shown to Emit Potentially Harmful Nanosized Particles," Atmospheric Environment.
<<https://phys.org/news/2013-07-3d-printers-shown-potentially.html>> 2013.
- [19] "MLab Cloud-hosted MongoDB," ObjectLabs Corporation, 2017. [Online]. Available: <https://mlab.com/>.
- [20] "SQLite self-contained SQL Database Engine," SQLite, 2005. [Online]. Available: <https://www.sqlite.org/>.
- [21] "aJson Arduino Library for JSON processing," Interactive Matter, Marcus Nowotny, 2010. [Online]. Available: <https://github.com/interactive-matter/aJson>.
- [22] "React, a JavaScript Library for building user interfaces," Facebook, Inc., 2017. [Online]. Available: <https://facebook.github.io/react/>.
- [23] "Bootstrap," Bootstrap., 2017. [Online]. Available: <http://getbootstrap.com/>.
- [24] "ReduxJS," Dan Abramov, 2017. [Online]. Available: <http://getbootstrap.com/>.
- [25] "Heroku Cloud Application Platform," Salesforce, Inc., 2017. [Online]. Available: <http://getbootstrap.com/>.